Input-specific learning rules at excitatory synapses onto hippocampal parvalbumin-expressing interneurons

Nicolas Le Roux, Carolina Cabezas, Urs Lucas Böhm, Jean Christophe Poncer

JPn Neuroscience
The Journal of Physiology

Input-specific learning rules at excitatory synapses onto hippocampal parvalbumin-expressing interneurons

Nicolas Le Roux[1,2,3], Carolina Cabezas[1,2,3,*], Urs Lucas Böhm[1,2,3,*] and Jean Christophe Poncer[1,2,3]

[1] *INSERM UMR-S 839, F75005, Paris, France*
[2] *Université Pierre et Marie Curie, F75005, Paris, France*
[3] *Institut du Fer à Moulin, F75005, Paris, France*
[*] *present address: ICM - Institut du Cerveau et de la Moelle épiniére, F75013, Paris, France*

Key points

- Parvalbumin-expressing interneurons represent a major source of inhibition of CA1 hippocampal principal cells and influence both spike timing precision and network oscillations.
- These interneurons receive both feed-forward and feedback excitatory inputs which recruit them in the hippocampal network.
- In this study, we compared the functional properties of these two inputs and how they may be modified by neuronal activity.
- We show that calcium-permeable AMPA receptors and NMDA receptors are differentially distributed at feed-forward *versus* feedback inputs and act as coincidence detectors of opposing modalities.
- Our results reveal that the two major excitatory inputs onto CA1 parvalbumin-expressing interneurons undergo long term plasticity with different frequency regimes of afferent activity, which is likely to influence their function under both normal and pathological conditions.

Abstract Hippocampal parvalbumin-expressing interneurons (PV INs) provide fast and reliable GABAergic signalling to principal cells and orchestrate hippocampal ensemble activities. Precise coordination of principal cell activity by PV INs relies in part on the efficacy of excitatory afferents that recruit them in the hippocampal network. Feed-forward (FF) inputs in particular from Schaffer collaterals influence spike timing precision in CA1 principal cells whereas local feedback (FB) inputs may contribute to pacemaker activities. Although PV INs have been shown to undergo activity-dependent long term plasticity, how both inputs are modulated during principal cell firing is unknown. Here we show that FF and FB synapses onto PV INs are endowed with distinct postsynaptic glutamate receptors which set opposing long-term plasticity rules. Inward-rectifying AMPA receptors (AMPARs) expressed at both FF and FB inputs mediate a form of anti-Hebbian long term potentiation (LTP), relying on coincident membrane hyperpolarization and synaptic activation. In contrast, FF inputs are largely devoid of NMDA receptors (NMDARs) which are more abundant at FB afferents and confer on them an additional form of LTP with Hebbian properties. Both forms of LTP are expressed with no apparent change in presynaptic function. The specific endowment of FF and FB inputs with distinct coincidence detectors allow them to be differentially tuned upon high frequency afferent activity. Thus, high frequency (>20 Hz) stimulation specifically potentiates FB, but not FF afferents. We propose that these differential,

 DOI: 10.1113/jphysiol.2012.245852

input-specific learning rules may allow PV INs to adapt to changes in hippocampal activity while preserving their precisely timed, clockwork operation.

(Received 5 October 2012; accepted after revision 16 January 2013; first published online 21 January 2013)
Corresponding author J. C. Poncer or N. Le Roux: INSERM UMR-S 839, 17 rue du Fer a Moulin, 75005 Paris, France. Email: jean-christophe.poncer@inserm.fr or nicolas.le-roux@inserm.fr

Abbreviations AMPA, (2-amino-3-(3-hydroxy-5-methyl-isoxazol-4-yl)propanoic acid); CP, calcium-permeable; FB, feedback; FF, feed-forward; INs, interneurons; LTP, long term potentiation; NMDA, *N*-methyl-D-aspartic acid; PPR, paired-pulse ratio; PV, parvalbumin.

Introduction

GABAergic inputs onto cortical principal neurons exert both a spatial and temporal control of their activity (Isaacson & Scanziani, 2011). GABAergic interneurons are recruited by excitatory inputs from principal neurons which in turn they inhibit. These excitatory afferents include feed-forward (FF) inputs made by long-range axons from different cortical areas or sub-regions and feedback (FB) inputs from neighbouring principal neurons. Inhibition recruited by FF and FB afferents effectively shapes principal cell activity in a different manner. Disynaptic, FF inhibition enforces precise temporal integration of excitatory inputs onto principal cells by shortening the time window of EPSP summation (Pouille & Scanziani, 2001; Isaacson & Scanziani, 2011). In contrast, FB inhibition scales GABAergic inhibition to local excitatory output, thereby contributing to the generation of rhythmic activities (Mann *et al.* 2005).

In the CA1 area, some GABAergic interneurons participate predominantly in either feed-forward (Pouille & Scanziani, 2001) or feedback (Maccaferri, 2005) inhibition. Parvalbumin-expressing interneurons (PV INs), however, fulfil both functions as they receive both FF afferents from Schaffer collaterals and perforant path and FB afferents from neighbouring principal cells (Takacs *et al.* 2012). These cells establish predominantly perisomatic contacts onto pyramidal neurons and are therefore well suited for controlling the discharge of their postsynaptic targets (Cobb *et al.* 1995; Pouille & Scanziani, 2001). In addition, their axonal divergence allows them to effectively synchronize large neuronal ensembles (Cobb *et al.* 1995). The efficacy of excitatory inputs onto PV INs greatly influences their spatial and temporal control over principal cell activity (Racz *et al.* 2009; Korotkova *et al.* 2010). Activity-dependent plasticity of synaptic strength at these synapses is then likely to be required to maintain the precisely timed operation of PV INs.

Although long thought to be intrinsically non-plastic (McBain *et al.* 1999), excitatory inputs onto hippocampal interneurons have recently been shown to undergo various forms of long-term, activity-dependent plasticity (Kullmann & Lamsa, 2007; Pelletier & Lacaille, 2008). Hebbian, NMDAR-dependent LTP has been observed at FF inputs onto some st. radiatum interneurons (Lamsa *et al.* 2005) and acts to maintain the temporal fidelity of synaptic integration in pyramidal cells. Another form of LTP depending on activation of calcium-permeable (CP-) AMPARs has been reported in several interneurons subtypes (Lamsa *et al.* 2007; Oren *et al.* 2009; Nissen *et al.* 2010; Szabo *et al.* 2012). Unlike NMDAR-dependent LTP, this form of plasticity requires coincident presynaptic activation and postsynaptic hyperpolarization and was thus named anti-Hebbian (Lamsa *et al.* 2007). Thus, opposing learning rules of excitatory inputs onto various interneurons subtypes seem to rely on the relative availability of synaptic NMDA *vs.* CP-AMPARs (Kullmann & Lamsa, 2007). However, whether this may apply to distinct inputs onto the same interneuron is unknown.

Here, we compared the functional and plastic properties of FF and FB excitatory inputs onto CA1 PV INs. We show these inputs exhibit distinct forms of long term potentiation that reflect a differential distribution of synaptic CP-AMPARs and NMDARs. These two forms of plasticity are induced by different regimes of afferent activity. Thus, distinct postsynaptic receptors at FF *vs.* FB inputs onto PV interneurons confer these inputs with differential frequency selectivity for long term, activity-dependent adaptation.

Methods

Animals

Pvalb$^{tm1(cre)Arbr}$ mice expressing Cre recombinase under the control of the *Pvalb* promoter (kindly provided by Dr Silvia Arber, University of Basel, Switzerland; Hippenmeyer *et al.* 2005) were crossed with *RCE:LoxP* reporter mice expressing enhanced green fluorescent protein (EGFP) under the control of promoter sequences for the Rosa locus enhanced with an additional CAG sequence (provided by Dr Gord Fishell, NYU, USA; Sousa *et al.* 2009). The genetic background of both *Pvalb*$^{tm1(cre)Arbr}$ and *RCE:LoxP* mice was C57Bl6(J). Homozygous, *PV*^{Cre}*::RCE* mice were used in all experiments. All the procedures carried out conformed to the International Guidelines on the ethical use of animals.

Electrophysiology

Horizontal hippocampal slices (300–350 μm thick) were prepared from postnatal day 17–23 PV^{Cre}::*RCE* mice as described (Scheuber *et al.* 2004). Mice were anesthetized by intraperitoneal injection of ketamine and xylazine (80 and 20 mg kg^{-1}, respectively) and killed by decapitation. The brain was quickly removed and immersed in low-sodium, ice-cold artificial CSF (low Na^+-ACSF) equilibrated with 95% O_2–5% CO_2. The composition of the low Na^+-ACSF was as follows: (in mM) 248 sucrose, 26 $NaHCO_3$, 10 glucose, 5 $MgCl_2$, 4 KCl, 1 $CaCl_2$, and 0.005‰ Phenol Red. After complete surgical (from st. lacunosum down to the alveus) transection between CA3 and CA1 areas to prevent propagation of recurrent excitation along Schaffer collaterals, slices were transferred to a submerged chamber maintained at 31°C, mounted on an upright microscope (BX51WI, Olympus France SA, Rungis, France) and superfused at 2.5 ml min^{-1} with ACSF composed of (in mM): 124 NaCl, 26.2 $NaHCO_3$, 11 D-glucose, 2.5 KCl, 1 NaH_2PO_4, 2 $CaCl_2$ and 3 $MgCl_2$.

Whole-cell patch-clamp recordings were made using borosilicate glass microelectrodes (3–5 MΩ resistance) filled with (in mM): 105 $CsMeSO_3$, 20 CsCl, 10 Hepes, 10 EGTA, 4 MgATP, 0.4 Na_3GTP (pH 7.4, 291 mosmol l^{-1}). For long term plasticity experiments, EGTA concentration was reduced to 0.1 mM and spermine was added to the internal solution to better preserve the voltage-dependent block of CP-AMPARs (Bowie & Mayer, 1995; Donevan & Rogawski, 1995; Koh *et al.* 1995). EPSCs were evoked at 0.1 Hz in the presence of bicuculline methochloride (20 μM) using ortho- or antidromic stimulation through monopolar glass microelectrodes placed either in st. radiatum to recruit feed-forward (FF) Schaffer collateral inputs and/or in st. oriens/alveus to recruit predominantly feedback (FB) inputs. Stimulation intensity and duration typically ranged 50–250 μA and 100–150 μs, respectively, for both interneuron and pyramidal cell recordings.

In most experiments (Fig. 2–5), synaptic plasticity was induced in voltage clamp by pairing 400 presynaptic stimuli delivered at 5 Hz with either continuous hyperpolarization to –90 mV (for anti-Hebbian conditioning) or depolarization to 0 mV (for Hebbian conditioning) (Lamsa *et al.* 2007). For all recordings, pairing was applied less than 10 min after break in (typically 5), in order to prevent washout of the intracellular milieu (Lamsa *et al.* 2007). In some experiments (Fig. 6), we tested the plasticity induced by various frequency regimes of afferent activity (900 pulses at 0.1, 1, 5 or 20 Hz (Dudek & Bear, 1992) or 100 pulses at 100 Hz repeated 5 times 10 s apart (Lamsa *et al.* 2005, 2007)). In these experiments, EPSCs were recorded in voltage-clamp mode, but the conditioning protocol was delivered in current clamp from resting membrane potential (-58.8 ± 0.4 mV for PV INs, -58.5 ± 1.3 mV for pyramidal cells). Neurons were therefore recorded with a potassium-based internal solution containing (in mM): 120 $KMeSO_3$, 10 KCl, 10 Hepes, 0.1 EGTA, 4 MgATP, 0.4 Na3GTP and 0.1 spermine (pH 7.4, 292 mosmol l^{-1}).

Glutamate uncaging onto individual PV+ INs was performed in the presence of 200–300 μM MNI-glutamate (Tocris Bioscience, Bristol, UK) together with bicuculline and tetrodotoxin using a 405 nm, laser diode beam (Deepstar, Omicron, Photon Lines, Saint-Germain-en-Laye, France) conducted through a multimode optic fibre and alignment device (Prairie Technologies, Middleton, WI, USA) set to generate a <3 μm spot in the objective focus. The power of the laser head output was controlled using Omicron Laser Controller v2.97, while trigger and pulse duration were set using Clampex and a Digidata controller. The stimulation site was set along the primary dendrite of a PV IN to obtain the fastest uEPSC onset kinetics with minimal laser intensity (2–20 mW) in order to minimize recruitment of extrasynaptic receptors. Pre-induction recordings were performed at 0.1 Hz with stimulation duration of 1.5 ms for at least 5 min. A pairing protocol was then applied, consisting of 100 pulses at 5 Hz while holding the cell at –90 mV. During the induction the stimulation duration was increased to 4 ms. uEPSCs were then recorded in the same conditions as prior to pairing for at least another 30 min.

Firing properties of PV INs were recorded in current-clamp mode using an internal solution containing (in mM): 120 $KMeSO_3$, 10 KCl, 10 Hepes, 0.1 EGTA, 4 MgATP and 0.4 Na_3GTP (pH 7.4, 292 mosmol l^{-1}). To generate firing frequency = f(current) curves, a range of depolarizing current pulses (0 to 0.6 nA) were delivered with an interstimulus interval of 2 s.

Signals were acquired and filtered at 10 kHz using a Multiclamp amplifier and digitized at 20 kHz using Clampex software (Molecular Devices, St. Grégoire, France). All parameters were analysed offline with Clampfit. Peak EPSC amplitudes were always measured between 1.8 and 2.8 ms of stimulation artefact to prevent contamination by disynaptic responses. Bicuculline, D,L-APV, Ro25-6981, DPCPX, NBQX were all purchased from Ascent Scientific (abcamBiochemicals, Cambridge, UK). Naspm was obtained from Tocris Bioscience.

Immunohistochemistry

P21 PV^{Cre}::*RCE* mice were rapidly anaesthetized by intraperitoneal injection of ketamine and xylazine (80 and 20 mg kg^{-1}, Sigma-Aldrich) and perfused transcardially with 4% (w/v) paraformaldehyde in 0.1 M sodium phosphate buffer, pH 7.5. Brains were post-fixed overnight in the same solution, stored at 4°C and cryoprotected

in 30% sucrose for an additional 48 h. Transverse, 40 μm-thick sections were cut with a cryotome (Microm KS34, Thermo Scientific Saint Herblain, France) and stored at −20°C in a solution containing 30% (v/v) ethylene glycol, 30% (v/v) glycerol, and 0.1 M sodium phosphate buffer, until they were processed for immunofluorescence. Free-floating sections were rinsed in PBS and then incubated for 1 h in PBS supplemented with 0.3% Triton X-100 and 5% normal goat serum. They were then incubated overnight at 4°C with primary antibodies. The following antibodies were used: GFP (polyclonal chicken, 1:1000, Chemicon, Millipore France SAS, Saint Quentin en Yvelines, France); PV (polyclonal rabbit, 1:1000, Swant, Marly, Switzerland). Sections were then rinsed in PBS and incubated for 1 h with donkey-FITC (1:500; all from Jackson Laboratory, Bar Harbor, ME, USA) and goat Cy3-coupled (1:600) secondary antibodies. Sections were rinsed in PBS and mounted with Mowiol/Dabco (25 mg ml^{-1}) and stored at 4°C before imaging.

Acquisition and analysis of images

Double-labelled images were obtained using fluorescence microscopy (DM6000; Leica Microsystems SAS, Nanterre, France) using × 10 and × 40 objectives. For estimating the proportion of GFP+ and PV+ cells, the entire CA1 was imaged in, at least, three different slices from each animal. The GFP+ and PV+ cells were counted manually.

Data are presented as means ± SEM. Statistical significance was assessed using a Mann–Whitney or Wilcoxon tests using SigmaStat (RITME, Paris, France). Principal component analysis (see online Supplementary material Fig. S1) was performed using Xlstat software (Addinsoft, Paris, France) under Microsoft Excel.

Results

In order to facilitate recordings from PV INs, we generated a mouse strain expressing EGFP specifically in these cells, by crossing *Pvalb*$^{tm1(cre)Arbr}$ mice (Hippenmeyer *et al.* 2005) with the sensitive reporter strain *RCE:LoxP* (Sousa *et al.* 2009). As expected from the delayed postnatal expression of PV in cortical interneurons (Solbach & Celio, 1991), EGFP was detected in hippocampal interneurons from homozygous *Pvalb*$^{tm1(cre)Arbr}$*::RCE:LoxP* mice (referred to as *PV*^{Cre}*::RCE* thereafter) from stages P7–P10. In area CA1, EGFP expression was detected in 93.0 ± 1.5% of PV-immunopositive neurons and 97.5 ± 0.3% EGFP-immunopositive interneurons were also immunopositive for PV (Supplementary Fig. S1*A* and *B*). Most (8 out of 11) neurons displayed fast spiking properties, short-lasting action potentials and fast AHP typical of hippocampal PV INs (Supplementary Fig. S1*C* and *D*). In addition, we could not distinguish subgroups of PV INs based on their intrinsic physiological properties (Supplementary Fig. S1*E* and *F*). Therefore, EGFP expression faithfully reflects PV expression and *PV*^{Cre}*::RCE* mice represent a valuable model for studying the physiology of hippocampal PV INs.

Distinct postsynaptic receptors at feed-forward *vs.* feedback excitatory inputs onto PV INs

Long term synaptic plasticity in hippocampal interneurons relies primarily on activation of Ca^{2+}-permeable postsynaptic glutamate receptors including GluA2-lacking AMPA receptors and NMDA receptors (Kullmann & Lamsa, 2007). Therefore we first compared the properties of EPSCs at feed-forward (FF) and feedback (FB) inputs onto CA1 PV INs. Whole-cell patch-clamp recordings were made from EGFP expressing cells with their soma within st. pyramidale in the CA1 area (Fig. 1*A*). EPSCs were evoked by focal stimulation either in st. radiatum to recruit FF inputs from Schaffer collaterals or in the st. oriens/alveus to recruit predominantly FB inputs from neighbouring CA1 pyramidal neurons (Takacs *et al.* 2012; Fig. 1*B*). Pharmacologically isolated AMPAR-mediated EPSCs evoked from either pathway onto PV INs showed pronounced, although not complete, inward rectification (Fig. 1*C* and *D*), suggesting they were carried predominantly by receptors lacking the GluA2 subunit. Consistent with this conclusion, AMPAR-mediated EPSCs in PV INs were partially blocked by the selective antagonist of Ca^{2+}-permeable (CP-) AMPARs, 1-Naphthyl acetyl spermine trihydrochloride (Naspm; Koike *et al.* 1997). Naspm (100 μM) reduced EPSC amplitude to a similar extent at FF and FB inputs onto PV INs (to 36.3 ± 3.3 and 40.0 ± 3.9% of control, respectively, $P = 0.6$, $n = 10$) but not at FF inputs onto principal cells (109.1 ± 5.2% of control, $n = 2$; Fig. 1*E* and *F*).

In hippocampal interneurons, synapses expressing CP-AMPARs classically display small NMDAR-mediated EPSC components (Lei & McBain, 2002; Kullmann & Lamsa, 2007; Lamsa *et al.* 2007). Quantitative immunogold studies have suggested that excitatory synapses onto hippocampal PV INs may even be largely devoid of NMDARs (Nyiri *et al.* 2003). Consistent with this observation, the NMDA/AMPA ratio of EPSCs evoked by Schaffer collateral stimulation in PV INs was considerably smaller than in neighbouring pyramidal cells (0.16 ± 0.02 *vs.* 1.23 ± 0.01; $P < 0.001$; Fig. 1*G*). However, this ratio was significantly greater for EPSCs evoked at FB compared to FF inputs onto PV INs (0.28 ± 0.04 *vs.* 0.16 ± 0.02, $P < 0.05$, $n = 12$ cells) but not pyramidal cells (1.11 ± 0.24 *vs.* 1.23 ± 0.01, $P = 0.6$, $n = 8$ cells). The amplitude of the NMDAR-mediated component of EPSCs evoked at distinct inputs onto CA3 interneurons has been correlated with their content in GluN2A and GluN2B subunits (Lei & McBain, 2002). We therefore asked whether the differential

contribution of NMDARs to EPSCs at FB *vs.* FF excitatory inputs onto PV INs may then reflect a similar difference in GluN2 subunit composition by comparing the effect of the specific GluN2B antagonist Ro25-6981. Application of 1 μM Ro25-6981 reduced NMDAR-mediated EPSCs to a similar extent at FB and FF inputs onto PV INs (-34 ± 12 *vs.* -37 ± 10% of control, $P = 0.9$, $n = 9$ cells; Fig. 1*H*). This effect, however, was more modest at excitatory synapses onto pyramidal cells (-17 ± 4% of control, $P = 0.07$, $n = 12$ cells). Thus, activation of both FB and FF excitatory synapses onto PV INs recruits GluA2-lacking AMPARs but NMDARs are more abundant at FB than at FF synapses.

Plasticity rules at FF *vs.* FB excitatory inputs onto PV interneurons

CP-AMPARs and NMDARs both act as coincidence detectors yet of opposing modalities. Ca^{2+} influx through the former is maximal during coincident glutamate

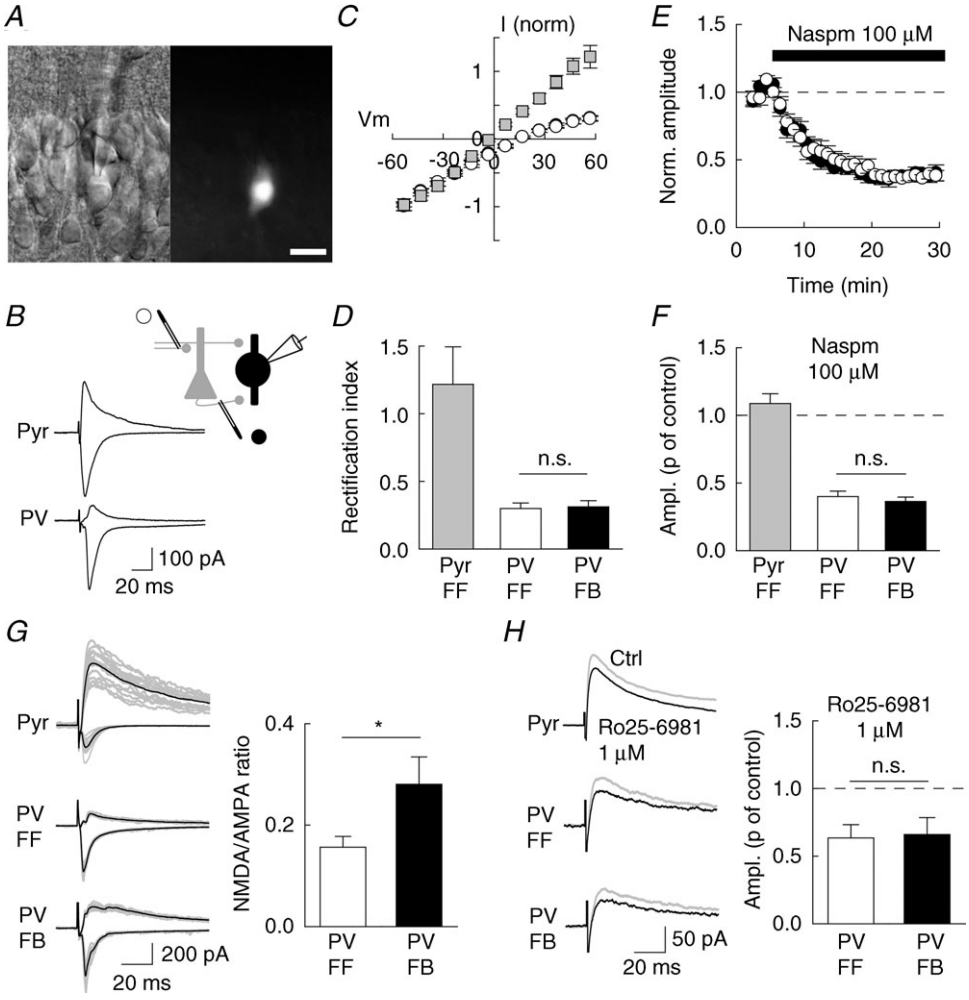

Figure 1. Postsynaptic receptor content at feed-forward *vs.* feedback excitatory inputs onto PV interneurons (INs)
A, infrared differential interference contrast (left) and fluorescence (right) video images of a CA1 GFP-expressing interneuron in an acute hippocampal slice from PV^{Cre}::*RCE* mouse. Scale, 20 μm. *B*, evoked EPSCs recorded at +60 mV or −60 mV for a pyramidal neuron (Pyr) and PV IN (PV) in the presence of 100 μM APV. *C* and *D*, current–voltage relation (*C*) and rectification index (*D*) of AMPAR-mediated EPSCs recorded from pyramidal neurons ($n = 4$, grey) or PV INs ($n = 7$) upon stimulation of either FF (white) or FB (black) afferents. *E*, time course of Naspm-induced partial block of EPSCs evoked in PV INs upon FF (white) or FB (black) afferent stimulation ($n = 10$). *F*, normalized EPSC amplitude upon 15–25 min of Naspm application. Mean data from 2 pyramidal neurons and 10 PV INs. *G*, left: 15 consecutive evoked EPSCs (grey) and mean currents (black) recorded at +60 mV or −60 mV for a pyramidal neuron (Pyr) and PV IN (PV). *G*, right: NMDA/AMPA ratio for EPSCs recorded from PV INs upon stimulation of FF (white) or FB (black) afferents ($n = 12$). *H*, left: NMDAR-mediated EPSCs recorded in the presence of 10 μM NBQX, before (grey) and after (black) application of Ro25-6981. *H*, right, normalized amplitude of the NMDA EPSC upon application of Ro25-6981 ($n = 5$). $^*P < 0.05$; n.s., non-significant.

release and postsynaptic hyperpolarization which both prevents channel blockade by endogenous polyamines and increases the driving force for Ca^{2+} ions. In contrast, Ca^{2+} influx through NMDARs requires coincident glutamate release and postsynaptic depolarization to relieve channel blockade by Mg^{2+} ions. We therefore asked whether the differential endowment of FF and FB inputs onto PV INs with postsynaptic receptors may influence plasticity rules at these synapses. We recorded EPSCs evoked by either FF or FB stimulation (at 0.1 Hz) before and after low-frequency pairing (400 pulses at 5 Hz) of only one pathway (Fig. 2). Two pairing modalities were tested: a Hebbian protocol consisting in pairing afferent stimulation with postsynaptic depolarization to 0 mV, and an anti-Hebbian protocol where presynaptic activation was paired with postsynaptic hyperpolarization to –90 mV (Lamsa *et al.* 2007). Anti-Hebbian pairing induced a persistent potentiation of both FF and FB inputs (+45.5 ± 14.5 and +38.8 ± 19.9% of control EPSC amplitude, respectively; $n = 11$ and 9 cells; Fig. 2*A* and *B*), which lasted for as long as recordings were maintained (>40 min). This form of potentiation was input specific as the other, unpaired pathway showed no significant plasticity (−2.6 ± 2.2 and +5.6 ± 1.2% on unpaired FB and FF inputs, respectively). In contrast, Hebbian pairing produced no long-lasting plasticity of FF inputs (+3.6 ± 6.2% of control EPSC amplitude) but a persistent potentiation of FB inputs (+38.4 ± 18.4%, $n = 8$; Fig. 2*C* and *D*). Thus, FF and FB excitatory inputs onto PV INs express two forms of LTP with opposing induction modalities which correlate with the differential expression of postsynaptic CP-AMPARs and NMDARs.

We therefore tested whether anti-Hebbian and Hebbian LTP induction in PV INs indeed relied on activation of CP-AMPARs and NMDARs, respectively. We used Naspm (100 μM) to partially block EPSCs immediately prior to delivering an anti-Hebbian pairing protocol and compared the recovery of the EPSC upon washing out Naspm in control *vs.* paired pathways (Fig. 3*A*). Naspm completely prevented anti-Hebbian LTP both at FF and FB inputs onto PV INs (Fig. 3*D*; $n = 6$ cells each). In contrast, application of APV (100 μM) did not block this form of plasticity (Fig. 3*C*; $n = 10$ and 11 cells, respectively) but abolished Hebbian LTP at FB inputs onto PV INs (Fig. 3*B* and *D*; $n = 14$ cells). These results demonstrate that in PV INs, two opposing forms of LTP are induced by activation of distinct postsynaptic receptor subtypes: anti-Hebbian LTP is mediated primarily by CP-AMPARs whereas Hebbian LTP relies on activation of NMDARs.

LTP expression in PV interneurons

We next examined the locus of LTP expression in PV INs using three independent approaches. We first tested whether LTP in PV INs was associated with changes in the short term plasticity of excitatory inputs. As previously reported in some unidentified basket or perisomatic CA2 and CA1 interneurons (Losonczy *et al.* 2002; Pouille & Scanziani, 2004), paired stimuli delivered 50 ms apart evoked EPSCs with a mean paired-pulse ratio (PPR) of 0.90 ± 0.05 at both FF and FB synapses ($n = 15$ and 24 cells, respectively), comparable to that described at unitary connections (Ali & Thomson, 1998; Mercer *et al.* 2012). The PPR of evoked EPSCs was not significantly changed upon anti-Hebbian LTP at FF (−4.9 ± 4.1%, $P = 0.6$, $n = 15$ cells) or FB synapses (−5.0 ± 2.9%, $P = 0.6$, $n = 14$ cells) or upon Hebbian LTP at FB synapses onto PV INs (−2.5 ± 3.0%, $P = 0.7$, $n = 10$ cells; Fig. 4*A* and *B*). These results suggest both forms of LTP may not primarily reflect changes in transmitter release.

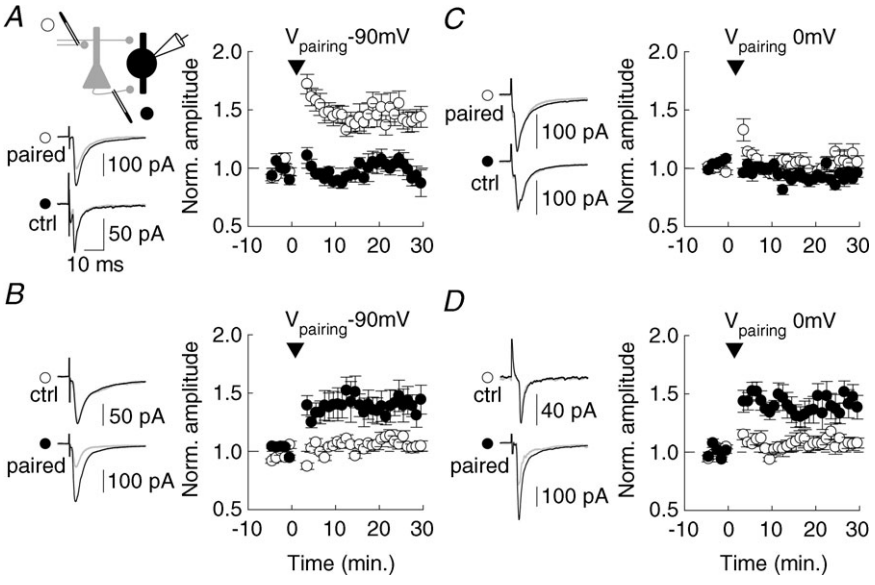

Figure 2. Distinct plasticity rules at FF *vs.* FB excitatory synapses onto PV INs
A–D, after a 5 min. control recording, afferent-specific stimulation (400 pulses at 5 Hz, arrowhead) was paired with either postsynaptic hyperpolarization to –90 mV (anti-Hebbian induction, *A, B*) or depolarization to 0 mV (Hebbian induction, *C, D*). Left, averaged EPSCs are shown for individual recordings before (grey) and after (black) pairing. Right, summary data from all experiments. Anti-Hebbian plasticity was observed at both FF (*A*, $n = 10$) and FB synapses (*B*, $n = 9$). However, Hebbian plasticity was induced only at FB (*D*, $n = 8$) but not FF (*C*, $n = 13$) synapses onto PV INs.

We next monitored the rate of EPSC suppression by the CP-AMPAR blocker Naspm as an index of release probability (Mainen *et al.* 1998). Inhibition of presynaptic A1 receptor is known to potentiate glutamatergic inputs onto hippocampal interneurons (Doherty & Dingledine, 1997). Application of the selective A1R antagonist DCPCX (100 μM) indeed potentiated EPSCs evoked at FF inputs onto PV INs by 43.3 ± 11.6% ($P < 0.01$, $n = 10$ cells; Fig. 4*C* and *D*). Subsequent application of Naspm produced a use-dependent block of EPSCs with a decay time constant of 3.5 ± 0.6 s ($n = 9$ cells), significantly faster than in interleaved, control experiments in the absence of DPCPX (5.5 ± 0.7 s, $P < 0.05$, $n = 17$ cells). Thus, a ∼40% potentiation of purely presynaptic origin at excitatory inputs on PV INs can be readily detected as an increase in the rate of Naspm-induced blockade of EPSCs. We then repeated the same experiment while comparing two independent FF inputs onto PV INs. Anti-Hebbian pairing of one pathway produced a 39.6 ± 8.5% increase in EPSC amplitude with no significant change in the other, control pathway (−4.4 ± 5.6%, $n = 21$ cells). Application of Naspm 15 min after pairing induced a blockade of EPSCs at a rate that was not significantly different between the two pathways ($P = 0.8$, $n = 21$ cells; Fig. 4*E* and *F*). Noticeably, the proportion of EPSC blocked by Naspm was also not significantly different between the potentiated and the control pathways (0.38 ± 0.05 *vs.* 0.43 ± 0.06 of control amplitude, respectively, $P = 0.5$). Together, these results strongly argue against LTP of excitatory inputs onto PV INs being expressed as a persistent change in release probability.

We therefore asked whether LTP of excitatory synapses onto PV INs could undergo long term plasticity independent of presynaptic function. We used laser-based, single-photon photolysis of MNI-glutamate (see Methods) to induce uncaging-evoked excitatory postsynaptic currents (uEPSCs) in EGFP+ PV INs. The position of the laser spot (≈ 3 μm in diameter) was adjusted along proximal dendrites in st. radiatum (20–40 μm from soma) to induce uEPSCs at 0.1 Hz that were fast rising and comparable in amplitude to mEPSCs (22.7 ± 2.2 *vs.* 18.3 ± 1.6 pA, $n = 11$ and 19 cells, respectively, $P = 0.1$; Fig. 5*A*). The peak amplitude and kinetics of uEPSCs were strongly dependent on subtle variations in the position of the laser (Fig. 5*B*), suggesting these currents might reflect activation of synaptic sites. Anti-Hebbian pairing (100 stimuli delivered at 5 Hz while holding the recorded cell at −90 mV) was then applied

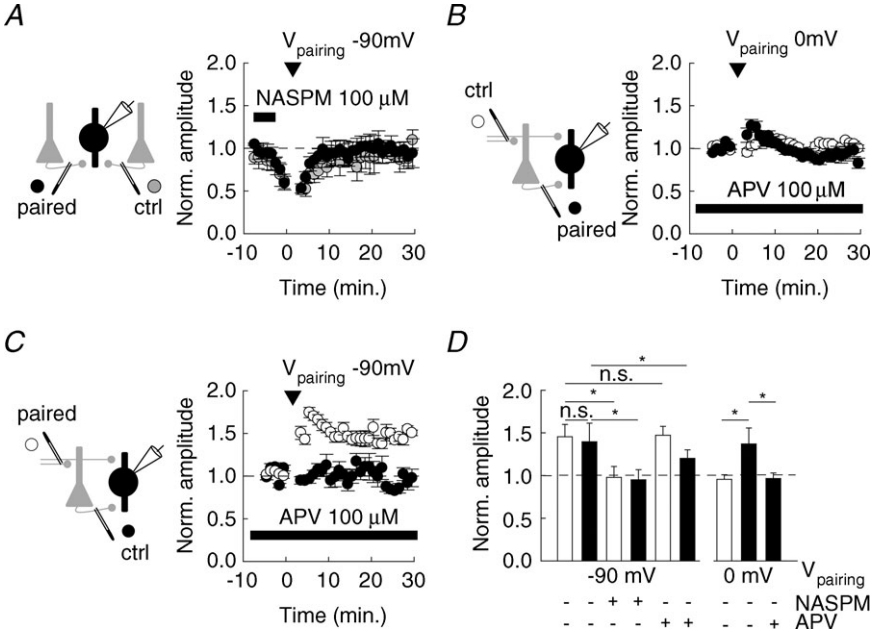

Figure 3. Anti-Hebbian and Hebbian LTP in PV INs require activation of GluA2-lacking AMPARs and NMDARs, respectively
A, application of Naspm (100 μM) immediately prior to pairing (arrowhead) prevented anti-Hebbian LTP at FB excitatory afferents ($n = 6$). Normalized EPSC amplitudes are shown for control (grey circles) and paired (black) pathways. No significant difference in the recovery of EPSCs from Naspm blockade was observed between control and paired pathways. *B*, *C*, application of 100 μM APV prevented the induction of Hebbian LTP at FB afferents (*B*, $n = 11$) without affecting induction of anti-Hebbian LTP at FF afferents (*C*, $n = 14$). *D*, summary data of all experiments showing the mean amplitude of EPSCs normalized to control upon Hebbian (0 mV) or anti-Hebbian (−90 mV) pairing in control conditions or in the presence of either Naspm or APV for FF (white) or FB (black) afferents. Changes in EPSC amplitude upon pairing are compared in the presence of antagonists *vs.* control conditions. *$P < 0.05$; n.s., non-significant.

within less than 10 min after break-in and led to a persistent (>30 min) potentiation of uEPSC amplitude ranging from 25 to 255% (average, $+83.2 \pm 27.9\%$ of control, $n = 8$ cells; Fig. 5*C* and *D*). Meanwhile, uEPSCs evoked at unpaired loci remained unaffected ($-4.3 \pm 3.6\%$ of control amplitude, $n = 3$ cells). Similarly, Hebbian pairing (same train of stimuli delivered while holding the cell at 0 mV) led to a persistent potentiation of uEPSC evoked by glutamate uncaging onto distal (>50 μm from soma, close to alveus border) but not proximal (20–40 μm from soma) dendrites in st. oriens ($+73.3 \pm 19.9\%$ of control, $n = 7$ cells, and $+3.5 \pm 10.1\%$ of control, $n = 6$ cells respectively, Fig. 5*E* and *F*). We conclude that excitatory synapses onto PV INs can undergo homosynaptic LTP that relies exclusively on post- but not presynaptic modifications.

Frequency dependence of long term plasticity at FF *vs.* FB inputs onto PV INs

Our results show that synaptic activation of CP-AMPARs and NMDARs underlie two forms of long term plasticity that are differentially induced at FF and FB inputs onto PV INs. Under which regimes of afferent activity may synaptic

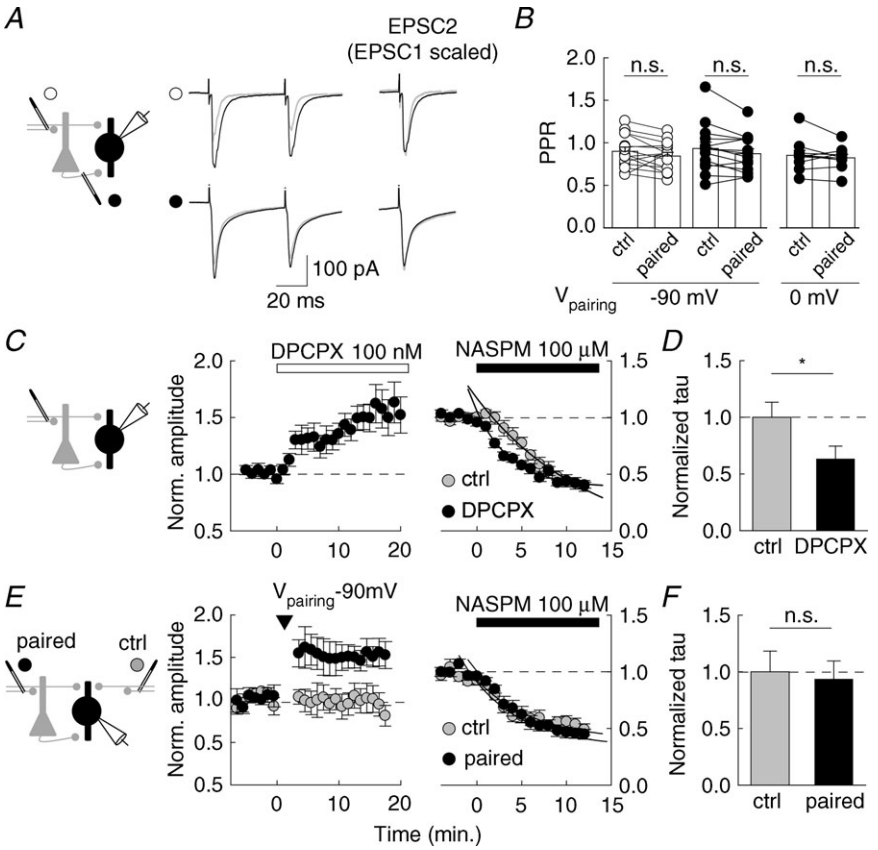

Figure 4. Presynaptic function is unaffected upon Hebbian and anti-Hebbian LTP in PV INs
A, averaged EPSCs evoked by paired pulses (50 ms apart) before (grey) and after (black) pairing-induced LTP. Top, anti-Hebbian LTP of FF inputs. Bottom, Hebbian pairing of FB inputs. Right, the second EPSC (EPSC2) is shown before and after pairing, after normalization to the peak amplitude of the first (EPSC1 scaled). No change in PPR was detectable in either condition. *B*, normalized PPR for control pathway or potentiated pathway. 5 Hz afferent stimulation was paired with hyperpolarization to −90 mV (FF inputs, white circles, $n = 15$; FB inputs, black circles, $n = 14$) or depolarization to 0 mV (FB inputs; black circles, $n = 10$). *C*, left: A1 receptor antagonist DPCPX (100 nM) increased EPSC amplitude in PV INs by about 40% ($n = 10$). *C*, right: compared effect of Naspm on evoked EPSCs in control conditions (grey circles, $n = 17$) or after potentiation by DPCPX ($n = 10$, black circles). EPSC amplitudes were normalized to mean values prior to Naspm application. The time course of Naspm-induced blockade of EPSCs (fitted to a single exponential) was faster in PV INs recorded in the presence of DPCPX. $^*P < 0.05$. *D*, summary data of the decay time constant (tau) of EPSC blockade by Naspm in either condition. *E*, *F*, similar experiment in which the effect of Naspm was monitored on EPSCs evoked from two independent FF pathways (paired, black circles; control, white circles). Arrowhead indicates pairing. EPSC amplitudes were normalized to values prior to Naspm application. No significant difference in the decay of EPSC amplitude was detected between the two pathways ($n = 10$).

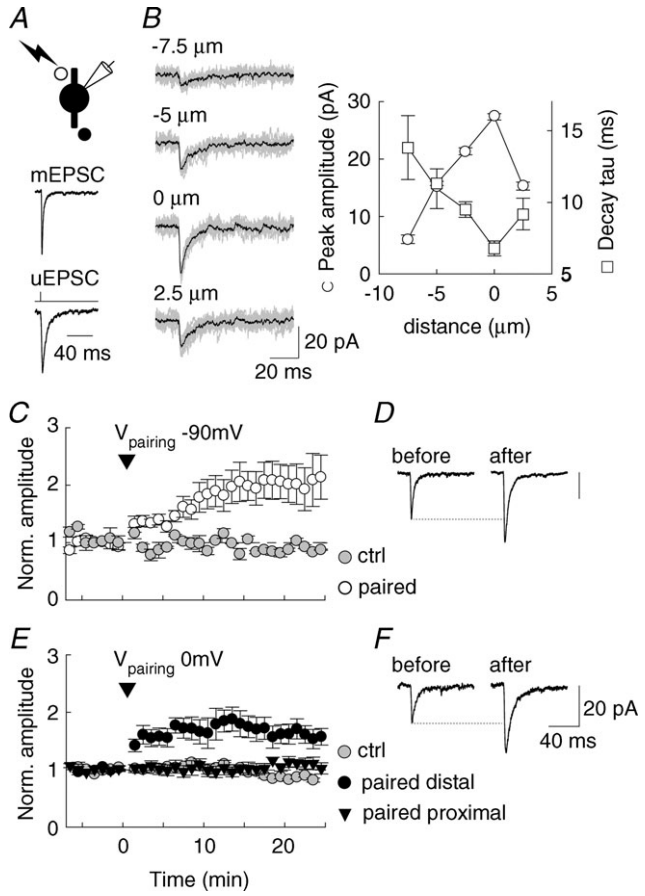

Figure 5. Postsynaptic Hebbian and anti-Hebbian LTP in PV INs
A, EPSCs evoked by focal uncaging of MNI-Glutamate onto proximal dendrites of PV INs in st. radiatum. Average of 30 uEPSCs normalized in amplitude and compared to 200 averaged mEPSCs recorded from the same cell showing fast onset kinetics despite slower decay of uEPSCs as compared to mEPSCs. *B*, right: uEPSCs evoked at various positions along a PV IN apical dendrite in st. radiatum. 10 individual uEPSCs (grey) are shown superimposed with averaged current (black) at each position. *B*, left, graph showing peak amplitude and decay time constant (decay tau) as a function of distance from the spot of maximal amplitude and minimal decay for the cell shown in right panel. Note the sharp decrease in amplitude and increase in decay kinetics of uEPSCs when light spot is moved away from optimal position. *C*, pairing consisting of 100 uEPSCs at 5 Hz with membrane hyperpolarization to –90 mV (arrowhead) leads to a persistent potentiation of uEPSC amplitude (white circles, $n = 8$ cells) as compared to control uEPSCs (grey circles, $n = 3$ cells). *D*, averaged uEPSCs from one such experiment before ($n = 30$) and 10–20 min after ($n = 40$) pairing. *E*, similar experiment on uEPSCs evoked by glutamate uncaging onto PV IN dendrites in st. oriens. Pairing of 100 uEPSCs at 5 Hz with membrane voltage clamped at 0 mV (arrowhead) leads to a potentiation of uEPSCs evoked at distal (>50 μm from soma close to alveus, black circles, $n = 7$ cells) but not proximal dendritic sites (20–40 μm from soma, black triangles, $n = 6$ cells) as compared to control (grey circles, $n = 3$ cells). *F*, averaged uEPSCs from one experiment with distally evoked uEPSCs before ($n = 30$) and 10–15 min after ($n = 40$) pairing.

efficacy at these inputs be selectively modified? During repetitive afferent activity, EPSP integration leads to a progressive depolarization of the postsynaptic membrane. This depolarization may lead to a frequency-dependent blockade of CP-AMPARs by endogenous polyamines whereas NMDAR activation may be facilitated due to relief of Mg^{2+} block. Thus, the sign and amplitude of CP-AMPAR- *vs.* NMDAR-dependent plasticity may be differentially influenced by the frequency of afferent stimulation (Dudek & Bear, 1992). We tested this hypothesis by comparing synaptic plasticity of FF and FB afferents onto PV INs induced by trains of afferent stimuli delivered at varying frequencies. Cells were held around their resting membrane potential in current-clamp mode and 1–100 Hz afferent stimulation was delivered to either FF or FB inputs (see Methods; Fig. 6). At frequencies up to 5 Hz, no summation of EPSPs was detected (Fig. 6*A* and *B*). At 100 Hz, however, summated EPSPs often depolarized PV INs above threshold, leading to the firing of action potentials (Fig. 6*D* and *E*). Unlike in pyramidal cells, low frequency stimulation did not lead to detectable LTD of excitatory inputs onto PV INs. However, 20 Hz stimulation induced a more pronounced LTP at synapses onto PV INs than that onto pyramidal cells ($P < 0.05$; Fig. 6*C* and *G*). Most strikingly, 100 Hz afferent stimulation led to a robust LTP of EPSCs both at Schaffer collateral synapses onto pyramidal cells ($+123 \pm 33\%$ of control, $n = 5$ cells) and FB inputs onto PV INs ($+144 \pm 42\%$ of control, $n = 5$ cells) whereas no potentiation was induced at FF inputs onto PV INs ($+5.3 \pm 17\%$ of control, $n = 7$ cells; Fig. 6*D* and *G*). We asked whether these distinct behaviours of FF and FB inputs upon 100 Hz stimulation reflected a differential recruitment of NMDA *vs.* CP-AMPARs. Application of 100 μM APV almost completely abolished the potentiation of EPSCs upon 100 Hz stimulation of FB afferents onto PV INs (to $+13.8 \pm 9.0\%$ of control, $n = 7$ cells; Fig. 6*E* and *G*), suggesting LTP at this frequency primarily relied on NMDAR activation. Conversely, 100 Hz stimulation of FF inputs induced a robust potentiation (to $+87.4 \pm 23.1\%$ of control, $n = 6$ cells; Fig. 6*F* and *G*) when delivered while holding PV INs at -90 mV to maximize Ca^{2+} influx through CP-AMPARs. Thus, our results show that the distinct endowment of excitatory synapses onto PV INs with various, calcium-permeable glutamate receptors accounts for a differential, long-term adaptation to specific frequency regimes of afferent activity.

Discussion

We have shown that distinct excitatory inputs onto CA1 PV INs exhibit different rules of long term plasticity depending on distinct postsynaptic receptors. The specific conditions required for CP-AMPAR and

NMDAR activation endow these inputs with a differential frequency selectivity of long term plasticity induction.

PV-expressing INs comprise several neuron subtypes targeting distinct membrane compartments on their post-synaptic targets. In particular, PV expression is found in basket and axo-axonic cells as well as in bistratified cells and, to a lesser extent, oriens-lacunosum moleculare (O-LM) cells (Klausberger & Somogyi, 2008). Since all recordings in this study were performed from PV INs with their soma within or close to st. pyramidale, it seems unlikely that O-LM cells were recorded. Although basket cells represent the majority of PV INs, we cannot exclude, however, the possibility that other PV INs were included in this study. In fact, three out of eleven PV INs did not show typical fast-spiking properties. Yet, no significant variability in the synaptic or plastic properties of PV INs was detected in this study. Thus, excitatory inputs onto various PV INs may share common plasticity rules or we may have oversampled one specific subtype of PV INs in our experiments. In the CA1 area, PV INs receive both FF and FB excitatory inputs. FF inputs include Schaffer collaterals from CA3 principal neurons as well as entorhinal inputs from the perforant path and inputs from the thalamus and the amygdala, whereas FB inputs originate from neighbouring pyramidal neurons (Klausberger & Somogyi, 2008). These inputs are

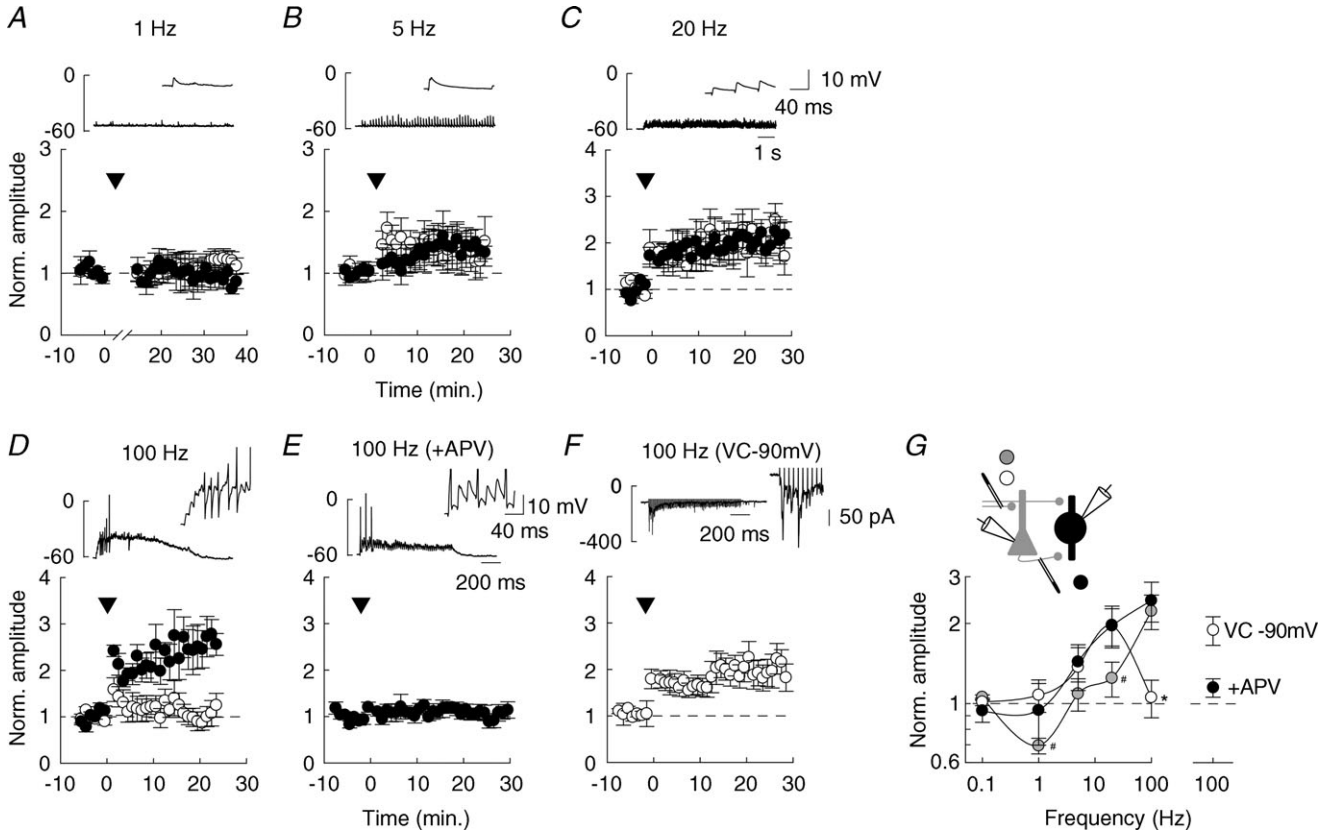

Figure 6. Frequency-dependent plasticity at FF *vs.* FB inputs onto PV INs
A–D, long term plasticity induced by repetitive afferent stimulation (arrowheads) to either FF (white) or FB (black) inputs onto PV INs. 900 pulses were delivered at 1 *(A)*, 5 *(B)* or 20 *(C)* Hz. In *D*, 100 pulses were delivered 5 times at 100 Hz while recording PV INs in current-clamp mode. Lower graphs represent averages of EPSC amplitudes recorded in voltage-clamp mode at –60 mV, normalized to control prior to conditioning stimulus; $n = 5$–7 cells for each frequency and each pathway. Upper graphs show sample recordings during conditioning stimulus at each frequency. Insets: detail of the first 150 ms. Note that 100 Hz stimulation only was sometimes sufficient to depolarize PV INs above firing threshold (action potentials are clipped due to filtering). *E*, 100 Hz stimulation was delivered to FB inputs in the presence of 100 μM APV to block NMDARs; $n = 7$ cells. *F*, 100 Hz stimulation was delivered to FF inputs while holding the postsynaptic cell to –90 mV in voltage-clamp (VC) mode to allow for activation of Ca^{2+}-permeable AMPARs; $n = 6$ cells. *G*, summary of all experiments with afferent stimulations delivered at various frequencies (1, 5, 20 or 100 Hz) at FF (white) or FB (black) inputs onto PV INs, or FF inputs onto pyramidal neurons (grey). Each data point represents the mean ± SEM of normalized EPSC amplitudes measured between 10 and 20 min after conditioning stimulus. Note that beyond 20 Hz stimulation, FF inputs onto PV INs show no LTP, in contrast to FB inputs and FF inputs onto pyramidal cells. $^{\#}P < 0.05$ FF inputs onto pyramidal cells compared to FF and FB inputs onto PV INs. $^{*}P < 0.05$ FF compared to FB inputs onto PV INs.

differentially segregated among the hippocampal layers such that most excitatory inputs in st. radiatum originate from Schaffer collaterals. Glutamatergic synapses in st. oriens/alveus are however more heterogeneous. Nevertheless, more than 50% recurrent CA1 excitatory inputs and less than 20% direct entorhinal inputs in this layer innervate local interneurons (Takacs *et al.* 2012). Therefore, although we cannot exclude that stimulation in st. oriens/alveus may have recruited glutamatergic synapses of various origins, it seems reasonable to assume that most of them originate from recurrent CA1 axons (Pouille & Scanziani, 2004). Thus, EPSCs evoked from st. radiatum and st. oriens/alveus in PV INs predominantly originate from FF and FB afferents, respectively.

Our results show that FF and FB inputs onto PV INs express different sets of postsynaptic glutamate receptors. AMPARs at excitatory inputs onto several hippocampal interneurons including PV INs have been described as predominantly lacking the GluA2 subunit (Leranth *et al.* 1996; Lamsa *et al.* 2007; Nissen *et al.* 2010). Consistent with these reports, we observed strong inward rectification of AMPAR-mediated EPSCs and partial block by the specific, GluA2-lacking AMPAR blocker Naspm. These properties were similar at FF and FB inputs onto PV INs and are likely to reflect a partial voltage-dependent blockade by endogenous cytoplasmic polyamines (Bowie & Mayer, 1995; Lamsa *et al.* 2007). NMDARs are instead differentially expressed at synapses from FF *vs.* FB excitatory inputs onto PV INs. EPSCs evoked upon stimulation of FF inputs are largely devoid of an NMDAR-mediated component. In contrast, EPSCs evoked at FB inputs show a significantly larger NMDA/AMPA ratio, although not as large as that of EPSCs recorded in principal neurons. Studies based on immunogold staining of the GluN1 subunit in rat hippocampus have revealed an almost complete absence of GluN1 at asymmetrical synapses onto PV IN dendrites (Nyiri *et al.* 2003). Interestingly, however, this observation was made on dendritic branches within st. radiatum. Instead, synapses established onto dendrites from unidentified interneurons within st. oriens showed an intermediate density of gold particles per synapses as compared to pyramidal cell dendrites and st. radiatum dendrites of PV INs (Nyiri *et al.* 2003). Thus, immunogold data and our present results converge to suggest a differential expression of GluN1 at FF *vs.* FB inputs onto PV INs. A similar, input-specific distribution of postsynaptic glutamate receptors has been observed in CA3 interneurons (Toth & McBain, 1998; Lei & McBain, 2002). However, in contrast to these cells, the synaptic CP-AMPAR content at synapses onto CA1 PV INs does not appear correlated with NMDAR content. The mechanisms that govern the selective targeting of NMDARs to FB inputs onto these cells now remain to be elucidated.

We report that AMPARs and NMDARs confer FF and FB inputs onto PV INs with distinct forms of long term plasticity. Both AMPAR- and NMDAR-mediated LTP have been reported at excitatory synapses onto CA1 hippocampal interneurons (Kullmann & Lamsa, 2007). However, either form of plasticity was usually observed in specific interneuron sub-populations. NMDAR-mediated LTP has been described primarily in st. radiatum interneurons mediating FF inhibition (Lamsa *et al.* 2005) whereas AMPAR-mediated LTP was observed in several interneuron subtypes (Oren *et al.* 2009; Nissen *et al.* 2010; Szabo *et al.* 2012) including at FB inputs onto CA1 PV INs (Nissen *et al.* 2010). In the latter experiments, however, NMDARs were pharmacologically blocked, thereby probably masking their contribution to Hebbian plasticity. Group I mGluRs have also been involved in the induction of both Hebbian (Perez *et al.* 2001) and anti-Hebbian (Le Duigou & Kullmann, 2011) forms of LTP in CA1 interneurons. Since PV INs express mGluR5 (van Hooft *et al.* 2000), we cannot exclude the possibility that these receptors may influence the forms of LTP we report. However, our experiments using Naspm demonstrate that specific activation of CP-AMPARs is strictly required for LTP induction using an anti-Hebbian protocol. Conversely, LTP induction with a Hebbian protocol strictly requires NMDAR activation.

CP-AMPARs and NMDARs are classically viewed as coincidence detectors of opposing modalities. Thus, membrane depolarization is required to relieve NMDAR channel blockade by Mg^{2+} ions (Nowak *et al.* 1984) whereas blockade of CP-AMPAR channels by endogenous polyamines is relieved by membrane hyperpolarization which also enhances the driving force for Ca^{2+} (Bowie & Mayer, 1995; Donevan & Rogawski, 1995). A protocol associating afferent stimulation and membrane hyperpolarization may then promote CP-AMPAR-mediated plasticity induction. This type of paradigm was named anti-Hebbian (Lamsa *et al.* 2007) as opposed to the classical Hebbian rule for plasticity induction. However, our experiments where LTP was induced in current-clamp mode reveal that membrane hyperpolarization is not required for induction of CP-AMPAR-mediated LTP. In fact, plasticity was readily induced around resting membrane potential up to 20 Hz afferent stimulation which led to significant depolarization due to EPSP summation. Thus, induction of long term plasticity mediated by CP-AMPARs does not strictly require membrane hyperpolarization or depolarization and may thus be called *non-Hebbian* rather than *anti-Hebbian*. Nevertheless, membrane potential influences plasticity rules at synapses expressing CP-AMPARs, in particular the frequency range of afferent activity that triggers plasticity (Fig. 6) and possibly the *modification threshold* as defined in the Bienenstock–Cooper–Munro formalism (Bienenstock *et al.* 1982; Bear *et al.* 1987).

Although the mechanisms of LTP in principal cells have been studied in exquisite detail (Malinow & Malenka,

2002; Poncer, 2003), LTP expression in hippocampal interneurons remains poorly understood. In O-LM interneurons, anti-Hebbian LTP has been suggested to be expressed presynaptically, based on concomitant changes in the coefficient of variation (CV) of the EPSPs (Oren *et al.* 2009). mGluR-dependent LTP in unidentified st. oriens interneurons on the other hand is associated with both reduced failure rate (Lapointe *et al.* 2004) and increased synaptic potency (Perez *et al.* 2001), suggestive of concomitant pre- and postsynaptic modifications. However, changes in both CV and failure rate may be erroneously attributed to presynaptic modifications (Poncer & Malinow, 2001). Our data argue against a presynaptic locus of LTP expression in CA1 PV INs. First, CP-AMPAR and NMDAR-mediated forms of LTP were not associated with a consistent increase in release probability, as detected either by changes in paired-pulse ratio or rate of Naspm-induced blockade of CP-AMPARs. Second, persistent LTP of uEPSCs could be induced by pairing glutamate uncaging onto st. radiatum or st. oriens/alveus dendrites of PV INs with either membrane hyperpolarization or depolarization, respectively (Fig. 5), suggesting both anti-Hebbian and Hebbian LTP may be induced through purely postsynaptic mechanisms in PV INs. Hence we suggest LTP in CA1 PV INs may be primarily expressed postsynaptically, possibly through an increase in postsynaptic receptor number or unitary conductance, as described in principal cells (Poncer, 2003). Although the mechanisms of such postsynaptic LTP expression remain to be elucidated, it is noteworthy that the fraction of AMPAR-mediated EPSC blocked by Naspm was unchanged after anti-Hebbian pairing (Fig. 4*E*). Therefore expression of this form of LTP at least may not involve changes in subunit composition of postsynaptic AMPARs (Plant *et al.* 2006).

Our data show that FF and FB excitatory inputs onto PV INs show distinct learning rules that rely on activation of different sets of postsynaptic receptors. These rules confer on FF and FB inputs a specific dependence on afferent activity frequency. Thus, at resting membrane potential, FF inputs are potentiated within a narrower frequency range of afferent activity frequency (5–20 Hz in our experimental conditions) than FB inputs (up to 100 Hz). How may these distinct learning rules influence network operation in the CA1 area? Even moderate changes in the excitatory drive of PV INs are sufficient to alter spike timing precision of PV INs with respect to gamma rhythm, reduce the power of gamma oscillations (Fuchs *et al.* 2007) and increase burst firing in principal cells (Racz *et al.* 2009). Therefore alterations of synaptic potency at excitatory inputs onto PV INs greatly influence their contribution to the generation of coordinated ensemble activities in the CA1 region. The net impact of the plasticity processes we describe here is likely to depend on PV IN subtypes, which comprise a majority of basket and chandelier cells as well as some bistratified cells (Klausberger & Somogyi, 2008). However, if we consider only basket and chandelier interneurons, these cells fire out of phase compared with principal neurons during theta oscillations (4–8 Hz). Our data predict that these conditions would favour expression of CP-AMPAR-mediated LTP at both FF and FB afferents. Since FF inhibition has been shown to be critical to ensure the temporal fidelity of principal cell discharge (Pouille & Scanziani, 2001), non-Hebbian LTP of FF inputs onto PV INs may then contribute to maintain this fidelity when excitatory inputs onto principal cells are potentiated (Lamsa *et al.* 2005). Conversely, firing of PV baskets cells is time locked with pyramidal cells during sharp waves ripples (SWRs; Klausberger & Somogyi, 2008) which may contribute to memory consolidation (Girardeau *et al.* 2009). During SWRs, large populations of CA3 and CA1 pyramidal neurons are entrained into brief but very high frequency oscillations (150–200 Hz). Our data predict that, although both FF and FB inputs onto PV baskets cells may be active during SWRs, FB inputs may undergo a selective potentiation through activation of NMDARs. Potentiated inputs may then contribute to improve spike timing precision of these cells during subsequent theta oscillations. In fact, specific ablation of NR1 in PV INs reduced theta and increased gamma oscillation power (Korotkova *et al.* 2010), an effect that remains unexplained mechanistically. It seems unlikely that NMDARs participate in phasic excitatory synaptic transmission onto PV INs. Instead, our data suggest NMDAR-dependent plasticity at FB inputs onto PV INs may be required to adjust their efficacy and maintain the precisely timed, clockwork control of PV INs over principal cell activity. Realistic models (Traub *et al.* 2003; Volman *et al.* 2011) will be needed to fully explore the functional consequences of input specific learning rules in various subtypes of hippocampal PV INs.

References

Ali AB & Thomson AM (1998). Facilitating pyramid to horizontal oriens-alveus interneurone inputs: dual intracellular recordings in slices of rat hippocampus. *J Physiol* **507**, 185–199.

Bear MF, Cooper LN & Ebner FF (1987). A physiological basis for a theory of synapse modification. *Science* **237**, 42–48.

Bienenstock EL, Cooper LN & Munro PW (1982). Theory for the development of neuron selectivity: orientation specificity and binocular interaction in visual cortex. *J Neurosci* **2**, 32–48.

Bowie D & Mayer ML (1995). Inward rectification of both AMPA and kainate subtype glutamate receptors generated by polyamine-mediated ion channel block. *Neuron* **15**, 453–462.

Cobb SR, Buhl EH, Halasy K, Paulsen O & Somogyi P (1995). Synchronization of neuronal activity in hippocampus by individual GABAergic interneurons. *Nature* **378**, 75–78.

Doherty J & Dingledine R (1997). Regulation of excitatory input to inhibitory interneurons of the dentate gyrus during hypoxia. *J Neurophysiol* **77**, 393–404.

Donevan SD & Rogawski MA (1995). Intracellular polyamines mediate inward rectification of Ca(2+)-permeable alpha-amino-3-hydroxy-5-methyl-4-isoxazolepropionic acid receptors. *Proc Natl Acad Sci U S A* **92**, 9298–9302.

Dudek SM & Bear MF (1992). Homosynaptic long-term depression in area CA1 of hippocampus and effects of N-methyl-D-aspartate receptor blockade. *Proc Natl Acad Sci U S A* **89**, 4363–4367.

Fuchs EC, Zivkovic AR, Cunningham MO, Middleton S, Lebeau FE, Bannerman DM, Rozov A, Whittington MA, Traub RD, Rawlins JN & Monyer H (2007). Recruitment of parvalbumin-positive interneurons determines hippocampal function and associated behavior. *Neuron* **53**, 591–604.

Girardeau G, Benchenane K, Wiener SI, Buzsaki G & Zugaro MB (2009). Selective suppression of hippocampal ripples impairs spatial memory. *Nat Neurosci* **12**, 1222–1223.

Hippenmeyer S, Vrieseling E, Sigrist M, Portmann T, Laengle C, Ladle DR & Arber S (2005). A developmental switch in the response of DRG neurons to ETS transcription factor signaling. *PLoS Biol* **3**, e159.

Isaacson JS & Scanziani M (2011). How inhibition shapes cortical activity. *Neuron* **72**, 231–243.

Klausberger T & Somogyi P (2008). Neuronal diversity and temporal dynamics: the unity of hippocampal circuit operations. *Science* **321**, 53–57.

Koh DS, Burnashev N & Jonas P (1995). Block of native Ca^{2+}-permeable AMPA receptors in rat brain by intracellular polyamines generates double rectification. *J Physiol* **486**, 305–312.

Koike M, Iino M & Ozawa S (1997). Blocking effect of 1-naphthyl acetyl spermine on Ca(2+)-permeable AMPA receptors in cultured rat hippocampal neurons. *Neurosci Res* **29**, 27–36.

Korotkova T, Fuchs EC, Ponomarenko A, von Engelhardt J & Monyer H (2010). NMDA receptor ablation on parvalbumin-positive interneurons impairs hippocampal synchrony, spatial representations, and working memory. *Neuron* **68**, 557–569.

Kullmann DM & Lamsa KP (2007). Long-term synaptic plasticity in hippocampal interneurons. *Nat Rev Neurosci* **8**, 687–699.

Lamsa K, Heeroma JH & Kullmann DM (2005). Hebbian LTP in feed-forward inhibitory interneurons and the temporal fidelity of input discrimination. *Nat Neurosci* **8**, 916–924.

Lamsa KP, Heeroma JH, Somogyi P, Rusakov DA & Kullmann DM (2007). Anti-Hebbian long-term potentiation in the hippocampal feedback inhibitory circuit. *Science* **315**, 1262–1266.

Lapointe V, Morin F, Ratte S, Croce A, Conquet F & Lacaille JC (2004). Synapse-specific mGluR1-dependent long-term potentiation in interneurones regulates mouse hippocampal inhibition. *J Physiol* **555**, 125–135.

Le Duigou C & Kullmann DM (2011). Group I mGluR agonist-evoked long-term potentiation in hippocampal oriens interneurons. *J Neurosci* **31**, 5777–5781.

Lei S & McBain CJ (2002). Distinct NMDA receptors provide differential modes of transmission at mossy fiber-interneuron synapses. *Neuron* **33**, 921–933.

Leranth C, Szeidemann Z, Hsu M & Buzsaki G (1996). AMPA receptors in the rat and primate hippocampus: a possible absence of GluR2/3 subunits in most interneurons. *Neuroscience* **70**, 631–652.

Losonczy A, Zhang L, Shigemoto R, Somogyi P & Nusser Z (2002). Cell type dependence and variability in the short-term plasticity of EPSCs in identified mouse hippocampal interneurones. *J Physiol* **542**, 193–210.

McBain CJ, Freund TF & Mody I (1999). Glutamatergic synapses onto hippocampal interneurons: precision timing without lasting plasticity. *Trends Neurosci* **22**, 228–235.

Maccaferri G (2005). Stratum oriens horizontal interneurone diversity and hippocampal network dynamics. *J Physiol* **562**, 73–80.

Mainen ZF, Jia Z, Roder J & Malinow R (1998). Use-dependent AMPA receptor block in mice lacking GluR2 suggests postsynaptic site for LTP expression. *Nat Neurosci* **1**, 579–586.

Malinow R & Malenka RC (2002). AMPA receptor trafficking and synaptic plasticity. *Annu Rev Neurosci* **25**, 103–126.

Mann EO, Suckling JM, Hajos N, Greenfield SA & Paulsen O (2005). Perisomatic feedback inhibition underlies cholinergically induced fast network oscillations in the rat hippocampus in vitro. *Neuron* **45**, 105–117.

Mercer A, Eastlake K, Trigg HL & Thomson AM (2012). Local circuitry involving parvalbumin-positive basket cells in the CA2 region of the hippocampus. *Hippocampus* **22**, 43–56.

Nissen W, Szabo A, Somogyi J, Somogyi P & Lamsa KP (2010). Cell type-specific long-term plasticity at glutamatergic synapses onto hippocampal interneurons expressing either parvalbumin or CB1 cannabinoid receptor. *J Neurosci* **30**, 1337–1347.

Nowak L, Bregestovski P, Ascher P, Herbet A & Prochiantz A (1984). Magnesium gates glutamate-activated channels in mouse central neurones. *Nature* **307**, 462–465.

Nyiri G, Stephenson FA, Freund TF & Somogyi P (2003). Large variability in synaptic N-methyl-D-aspartate receptor density on interneurons and a comparison with pyramidal-cell spines in the rat hippocampus. *Neuroscience* **119**, 347–363.

Oren I, Nissen W, Kullmann DM, Somogyi P & Lamsa KP (2009). Role of ionotropic glutamate receptors in long-term potentiation in rat hippocampal CA1 oriens-lacunosum moleculare interneurons. *J Neurosci* **29**, 939–950.

Pelletier JG & Lacaille JC (2008). Long-term synaptic plasticity in hippocampal feedback inhibitory networks. *Prog Brain Res* **169**, 241–250.

Perez Y, Morin F & Lacaille JC (2001). A hebbian form of long-term potentiation dependent on mGluR1a in hippocampal inhibitory interneurons. *Proc Natl Acad Sci U S A* **98**, 9401–9406.

Plant K, Pelkey KA, Bortolotto ZA, Morita D, Terashima A, McBain CJ, Collingridge GL & Isaac JT (2006). Transient incorporation of native GluR2-lacking AMPA receptors during hippocampal long-term potentiation. *Nat Neurosci* **9**, 602–604.

Poncer JC (2003). Hippocampal long term potentiation: silent synapses and beyond. *J Physiol Paris* **97**, 415–422.
Poncer JC & Malinow R (2001). Postsynaptic conversion of silent synapses during LTP affects synaptic gain and transmission dynamics. *Nat Neurosci* **4**, 989–996.
Pouille F & Scanziani M (2001). Enforcement of temporal fidelity in pyramidal cells by somatic feed-forward inhibition. *Science* **293**, 1159–1163.
Pouille F & Scanziani M (2004). Routing of spike series by dynamic circuits in the hippocampus. *Nature* **429**, 717–723.
Racz A, Ponomarenko AA, Fuchs EC & Monyer H (2009). Augmented hippocampal ripple oscillations in mice with reduced fast excitation onto parvalbumin-positive cells. *J Neurosci* **29**, 2563–2568.
Scheuber A, Miles R & Poncer JC (2004). Presynaptic Cav2.1 and Cav2.2 differentially influence release dynamics at hippocampal excitatory synapses. *J Neurosci* **24**, 10402–10409.
Solbach S & Celio MR (1991). Ontogeny of the calcium binding protein parvalbumin in the rat nervous system. *Anat Embryol (Berl)* **184**, 103–124.
Sousa VH, Miyoshi G, Hjerling-Leffler J, Karayannis T & Fishell G (2009). Characterization of Nkx6–2-derived neocortical interneuron lineages. *Cereb Cortex* **19** (suppl 1), i1–10.
Szabo A, Somogyi J, Cauli B, Lambolez B, Somogyi P & Lamsa KP (2012). Calcium-permeable AMPA receptors provide a common mechanism for LTP in glutamatergic synapses of distinct hippocampal interneuron types. *J Neurosci* **32**, 6511–6516.
Takacs VT, Klausberger T, Somogyi P, Freund TF & Gulyas AI (2012). Extrinsic and local glutamatergic inputs of the rat hippocampal CA1 area differentially innervate pyramidal cells and interneurons. *Hippocampus* **22**, 1379–1391.
Toth K & McBain CJ (1998). Afferent-specific innervation of two distinct AMPA receptor subtypes on single hippocampal interneurons. *Nat Neurosci* **1**, 572–578.
Traub RD, Pais I, Bibbig A, LeBeau FE, Buhl EH, Hormuzdi SG, Monyer H & Whittington MA (2003). Contrasting roles of axonal (pyramidal cell) and dendritic (interneuron) electrical coupling in the generation of neuronal network oscillations. *Proc Natl Acad Sci U S A* **100**, 1370–1374.
van Hooft JA, Giuffrida R, Blatow M & Monyer H (2000). Differential expression of group I metabotropic glutamate receptors in functionally distinct hippocampal interneurons. *J Neurosci* **20**, 3544–3551.
Volman V, Behrens MM & Sejnowski TJ (2011). Downregulation of parvalbumin at cortical GABA synapses reduces network gamma oscillatory activity. *J Neurosci* **31**, 18137–18148.

Author contributions

J.C.P. and N.L.R. designed the research. C.C. contributed to establishing PV^{Cre}*::RCE* mice and performed some preliminary experiments. N.L.R. and U.L.B. performed the research. N.L.R. and J.C.P. analysed the data and wrote the paper. All authors approved the final version of the manuscript.

Acknowledgements

We thank S. Arber and G. Fishell for kindly providing $Pvalb^{tm1(cre)Arbr}$ and *RCE:LoxP* mice, T. Irinopoulou for assistance with imaging, M. Mameli for helpful discussions and R. Miles and M. Mameli for critical reading of the manuscript. This work was supported by the Institut National de la Santé et de la Recherche Médicale (Avenir program grant to J.C.P.), Ecole des Neurosciences de Paris (fellowship to U.L.B.), research grants (to J.C.P.) from the City of Paris, the Fyssen Foundation and the Agence Nationale de la Recherche. The authors declare no conflict of interest.